Strain-driven electric control of magnetization reversal at multiferroic interfaces

Dorj Odkhuu and Nicholas Kioussis

Phys. Rev. B **97**, 094404 — Published 2 March 2018

DOI: 10.1103/PhysRevB.97.094404

Strain Driven Electric Control of Magnetization Reversal at Multiferroic Interfaces

Dorj Odkhuu[1,2,*] and Nicholas Kioussis[1,†]

[1]*Department of Physics, California State University, Northridge, CA 91330, USA*
[2]*Department of Physics, Incheon National University, Incheon 22012, South Korea*

(Dated: February 20, 2018)

We predict that biaxial strain of several percent has a colossal effect on the magnetic anisotropy of ultrathin Fe/$XTiO_3$ (X=Sr, Ba) bilayers grown epitaxially on appropriate substrates. We demonstrate for the first time that under large compressive biaxial strain the Fe film undergoes an in- to out-of-plane spin reorientation via ferroelectric polarization switching, where the critical strain depends on the Fe film thickness. The underlying mechanism is the interplay between the strain-enhanced magnetoelectric coupling associated with the enhanced polarization in the ferroelectric substrate and the strain-reduced magnetic anisotropy energy of the Fe overlayer. These findings open interesting prospects for exploiting stain engineering to harvest higher electric field efficiency of magnetic anisotropy for the next generation of MeRAM devices.

PACS numbers: 75.70.Cn, 73.20.Hb, 73.20.-r, 77.55.Nv

I. INTRODUCTION

Multifunctionality in magnetoelectric (ME) materials, which simultaneously possess several ferroic [ferromagnetic, ferroelectric, and ferroelastic] orders, gives rise to novel physical phenomena and offers great opportunities for new device functions [1–3]. The coupling between the various degrees of freedom allows control of one order via the conjugate field associated with a different ferroic order [4]. Of particular interest is the control of magnetism by an electric field [5, 6], as opposed to current-driven magnetization switching via the spin transfer torque [7, 8], which can lead to a new paradigm of ultra-low power, highly scalable, and nonvolatile magnetoelectric random access memory (MeRAM) [9–11].

In contrast to single-phase multiferroics (MFs) and MEs which display a weak polarization-magnetization coupling, two-phase artificial systems, consisting of magnetostrictive [ferromagnetic (FM)] thin films grown epitaxially on piezoelectric [ferroelectric (FE)] substrates, exhibit more robust ME effect at room-temperature [12, 13]. This effect is mediated by the electric-field-driven strain in the piezoelectric constituent which is mechanically transferred to the magnetostrictive component, altering its magnetic properties [14–17].

The strain imparted in the FM/FE interface can mediated through (a) mismatch in lattice parameter between the FE film and the underlying substrate on which the FE is grown epitaxially [18–23], and (b) an electric field due to the inverse piezoelectric effect of the FE and the polarization switching (sensitivity of atomic displacements at the interface on polarization direction) [14, 15]. For example, even though the cubic $SrTiO_3$(STO) is not FE, under biaxial compressive (tensile) strain due to the underlying $(LaAlO_3)_{0.29}(SrAl_{0.5}Ta_{0.5}O_3)_{0.71}$ ($DyScO_3$) substrate it becomes ferroelectric with an out-of-(in-) plane polarization [19, 22]. Similar tuning of ferroelectric properties (spontaneous polarizations, Curie temperature, and piezoelectric coefficients) has been reported in biaxially strained $BaTiO_3$(BTO) [18, 23] and $PbTiO_3$ [20, 24] FE thin films to match the underlying substrate. Furthermore, the persistence of ferroelectricity down to nanometer-thick films was confirmed theoretically [25] and experimentally [26–28].

Previous *ab initio* calculations [14, 29–33] of FM/FE interfaces examined solely the electric-field-driven magnetoelastic effect (effect (b)) on the magnetization and on the magnetic anisotropy energy (MAE). These calculations show that the interface magnetoelectric coefficient, $\alpha_s = \mu_0(\Delta M_s/A)/E$, is about 2×10^{-9} G cm^2 V^{-1}, where, $\Delta M_s/A$, is the change of the interface magnetization per unit area and E is the external field, which often is taken to be the coercive field, E_c, at which the polarization can be switched. Furthermore, the calculations find a small change of MAE upon polarization reversal and none of them was able to show a spin reorientation upon polarization switching. On the other hand, for sufficiently thin films, huge biaxial strains (effect (a)) of several percent can be tolerated [18–20], which are much larger than those of ~ 0.1–0.2 % induced by an electric field. This mechanism, which is very different than the interface bond reconfiguration, remains unexplored thus far.

The objective of this work is to employ *ab initio* electronic structure calculations to investigate the effect of the giant biaxial strain imparted on the Fe/STO and Fe/BTO interfaces via a suitable underlying substrate on the magnetic properties of ultrathin Fe overlayers. The calculations reveal that the strain-induced enhancement of the polarization increases the interface ME effect and tunes the MAE depending on the direction of polarization. This in turn leads to a strain-driven out-of- to in-plane spin reorientation by switching the ferroelectric polarization. Through the analysis of the spin-orbit Hamiltonian matrix elements we elucidate the underlying mechanism for magnetization reversal in terms of the strain- and polarization-reversal-induced changes in the spin-orbit coupled d states of the interfacial Fe atom.

II. COMPUTATIONAL DETAILS

We use density-functional theory (DFT) calculations within the projector augmented-wave method [34], as implemented in the Vienna *ab initio* simulation package (VASP) [35, 36].

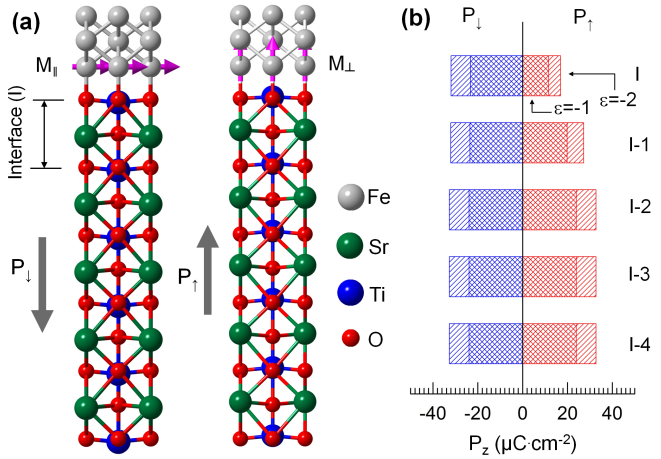

FIG. 1: (Color online) (a) Atomic structure of the (001) Fe/$SrTiO_3$ bilayer consisting of three monolayers of Fe on five unit cells of $SrTiO_3$ under –2% compressive strain. Gray, green, blue, and red spheres denote the Fe, Sr, Ti, and O atoms, respectively. The pink horizontal (vertical) arrows for the interfacial Fe atoms denote the in-plane (out-of-plane) magnetization orientation for down (up) polarization direction. (b) Calculated out-of-plane local polarization, P_z, for the Ith unit cell (I denotes the interface) for $P_\downarrow$ (blue bars)and $P_\uparrow$ (red bars) under –1% and –2% biaxial strain, respectively.

The generalized gradient approximation (GGA) is used to describe the exchange-correlation functional as parametrized by Perdew *et al.* [37]. The slab supercell for the Fe/STO (BTO) bilayer along [001], shown in Fig. 1(a), consists of three monolayers (MLs) of bcc Fe on top of fifteen MLs (five unit cells (uc)) of STO or BTO and a 15 Å-thick vacuum region separating the periodic slabs. The <110> axis of bcc Fe is aligned with the <100> axis of the BTO or STO where the O atoms of the TiO_2-terminated interface placed atop of Fe atoms [14]. We used an energy cutoff of 500 eV and a 15×15×1 Brillouin zone k-point mesh to relax the structures until the largest force becomes less than 10^{-2} eV/Å and the change in the total energy between two ionic relaxation steps is smaller than 10^{-5} eV. More specifically, for each epitaxial strain the ionic positions of the Fe layers and the two $SrTiO_3$ ($BaTiO_3$) unit cells near the interface were relaxed while those for the three bottom-most $SrTiO_3$ ($BaTiO_3$) unit cells were kept frozen at their relaxed bulk positions to retain the bulk polarization. The calculated equilibrium in-plane bulk lattice constants, a_0, of 3.95 Å and 4.00 Å for STO and BTO, respectively, agree with the experimental values of 3.905 and 4.00 Å respectively, where the GGA overestimates the lattice constant of STO by about 1.1% [23]. Consequently, there is a lattice mismatch between the Fe overlayer and the STO (BTO) substrate of about 1.3% (∼0%). The spin-orbit coupling (SOC) of the valence electrons is in turn included using the second-variation method [38] employing the scalar-relativistic eigenfunctions of the valence states and a 31×31×1 k-point mesh.

TABLE I: Values of the c/a ratio and the polarization P (μC cm^{-2}) along the c-axis for bulk $SrTiO_3$ and $BaTiO_3$, respectively, under different values of biaxial compressive strain.

	$SrTiO_3$		$BaTiO_3$	
ε	c/a	P_z	c/a	P_z
0	1.00 (1.00)[a]	0.0 (0.0)[b]	1.04 (1.02)[c]	28.9 (26)
–1	1.03 (1.02)[a]	23.9 (20) [b]	1.08 (1.03)[c]	34.8 (37)[c]
–2	1.05	32.7 (28)[b]	1.12 (1.06)[c]	41.5 (43)[c]
–3	–	–	1.16	55.6

[a]Reference[22]
[b]Reference[39]
[c]Reference[23]

III. RESULTS AND DISCUSSION

The calculated c/a ratio and the bulk polarization along [001] as a function of the in-plane biaxial compressive strain $\varepsilon = (a_\parallel - a_0)/a_0 \times 100\%$, for bulk STO and BTO are summarized in Table I and compared with experiment [22, 23] and previous theoretical calculations [21, 39], where the agreement overall is very good. The spontaneous polarization is calculated using the Berry phase approach for determining the electronic contribution to the polarization [40].

In Table II we show the c/a ratio and the relative displacements of the Ti ($d_{\text{Ti-O}}$) and Fe ($d_{\text{Fe-O}}$) atoms with respect to the O's at the interface for ferroelectric polarization pointing down ($P_\downarrow$) and up ($P_\uparrow$) for the Fe/STO and the Fe/BTO bilayers, respectively, under different values of biaxial strain. Here, positive (negative) $d_{\text{Ti-O}}$ denotes a Ti displacement towards (away from) the Fe layers. For $P_\uparrow$ both the c/a ratio and $d_{\text{Ti-O}}$ are reduced relative to the bulk values due to the presence of the Fe layers, while they remain the same as those in bulk for $P_\downarrow$. The optimized $d_{\text{Fe-O}}$ values of 1.94 and ∼1.92 Å for the unstrained Fe/STO and Fe/BTO, respectively, are smaller than those in bulk FeO (2.145 Å) [41] resulting in substantial interface effects of the electric depolarization and orbital hybridization [14, 29–33]. For both Fe/STO and Fe/BTO bilayers, $d_{\text{Fe-O}}$ increases slightly with strain but is almost polarization-independent. The interlayer distances, $d_{\text{Fe(I)-Fe(C)}}$ and $d_{\text{Fe(C)-Fe(S)}}$, between the three Fe layers under the polarization reversal are also shown in Table II for different strains, where the letters I, C, and S denote the interface, central, and surface layer, respectively. The out-of-plane lattice constant (2.93 Å) of the Fe film of the unstrained Fe/STO bilayer is enhanced relative to its bulk value (2.87 Å) due to the epitaxial strain, while the bulk lattice constant is almost preserved for the Fe/BTO bilayer. Both $d_{\text{Fe(I)-Fe(C)}}$ and $d_{\text{Fe(C)-Fe(S)}}$ increase with strain, leading to a significant tetragonal distortion of the Fe unit cell.

Table III presents the magnetic spin moments, μ_s^X (X=Fe, Ti), of the interfacial Fe and Ti atoms for the Fe/STO and the Fe/BTO bilayers, respectively, under different values of biaxial strain. We also list values of the orbital moment difference, $\Delta\mu_o = \mu_o^{[100]} - \mu_o^{[001]}$, and the change of the total

TABLE II: Values of the c/a ratio, the relative displacements of the Ti ($d_{\text{Ti-O}}$) and Fe ($d_{\text{Fe-O}}$) atoms with respect to the O-plane at the interface, and the interlayer distances, $d_{\text{Fe(I)-Fe(C)}}$ and $d_{\text{Fe(I)-Fe(C)}}$, between the Fe layers for down and up polarization and for different values of biaxial strain for the Fe/$SrTiO_3$ and Fe/$BaTiO_3$ bilayers, respectively. The letters I, C, and S denote the interface, central, and surface layer, respectively.

ε	$c/a(P_\downarrow)$	$c/a(P_\uparrow)$	$d_{\text{Ti-O}}(P_\downarrow)$	$d_{\text{Ti-O}}(P_\uparrow)$	$d_{\text{Fe(I)-O}}(P_\downarrow)$	$d_{\text{Fe(I)-O}}(P_\uparrow)$	$d_{\text{Fe(I)-Fe(C)}}(P_\downarrow)$	$d_{\text{Fe(I)-Fe(C)}}(P_\uparrow)$	$d_{\text{Fe(C)-Fe(S)}}(P_\downarrow)$	$d_{\text{Fe(C)-Fe(S)}}(P_\uparrow)$
$SrTiO_3$										
0	0.998	0.998	–0.003	–0.003	1.940	1.940	1.536	1.536	1.396	1.396
–1	1.026	1.020	–0.126	0.070	1.957	1.951	1.561	1.554	1.420	1.417
–2	1.054	1.032	–0.181	0.095	1.968	1.964	1.580	1.561	1.452	1.450
$BaTiO_3$										
0	1.047	1.034	–0.168	0.076	1.928	1.919	1.522	1.512	1.354	1.352
–1	1.079	1.058	–0.210	0.098	1.938	1.932	1.539	1.522	1.397	1.393
–2	1.131	1.089	–0.255	0.124	1.946	1.940	1.560	1.541	1.423	1.420
–3	1.194	1.128	–0.313	0.168	1.965	1.958	1.579	1.557	1.451	1.449

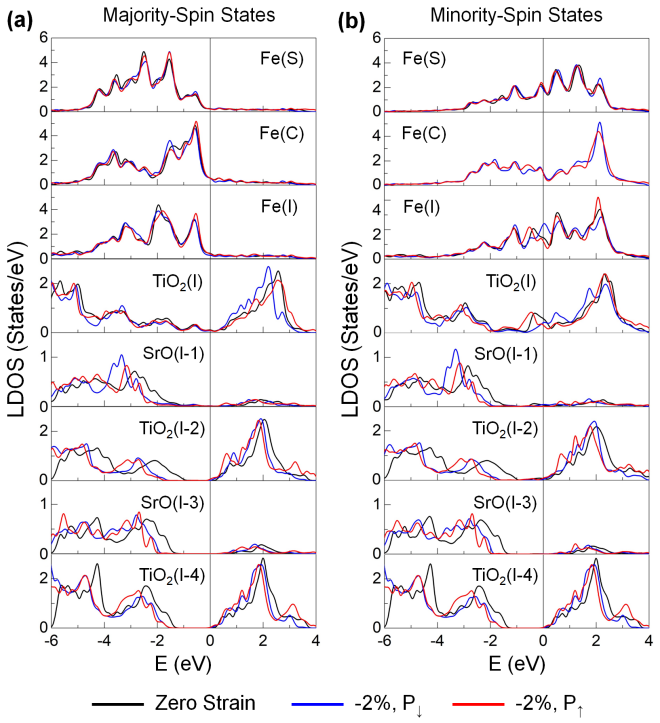

FIG. 2: (Color online) (a) Majority-spin and (b) minority-spin LDOS of the Fe/$SrTiO_3$ bilayer for down and up polarization under zero (black curve) and -2% strain (blue and red curves). The letters *I*, *C*, and *S* denote the interface, central, and surface layer, respectively. The Fermi level is set at zero energy.

interfacial spin moment, $\Delta\mu_s = \Delta\mu_s^{\text{Fe}} + \Delta\mu_s^{\text{Ti}}$, upon polarization reversal which is a measure of the interface magnetoelectric effect, α_s. For the unstrained Fe/STO (Fe/BTO) bilayer the interfacial Fe atom has a magnetic moment of 2.67 μ_B (2.76 μ_B for $P_\downarrow$ and 2.65 μ_B $P_\uparrow$), while the central and surface atoms have magnetic moments of ∼2.34 μ_B and ∼2.90 μ_B, respectively. The induced magnetic moment of the interfacial Ti atom of –0.34 μ_B (–0.45 μ_B for $P_\downarrow$ and -0.53 μ_B $P_\uparrow$) is antiparallel to the Fe moment consistent with previous *ab initio* calculations [14]. The change of the magnetic moment, $\Delta\mu_s^X = \mu_s^X(P_\downarrow) - \mu_s^X(P_\uparrow)$, upon polarization switching increases with biaxial compressive strain for both the interfacial Ti and Fe atoms, indicating a strain-induced large enhancement of the magnetoelectric coupling. Our value of the interfacial Fe magnetic moment agrees well with that of ∼2.6 μ_B reported in Ref. [14]. On the other hand, even though our interfacial Fe magnetic moment does not agree with the rather low value of ∼1 μ_B reported in Refs. [42, 43] the change of interfacial Fe moment, $\Delta\mu_s^{Fe}$ = 0.09 μ_B, upon polarization reversal is in good agreement. Presumably, the difference in the interfacial Fe moment may be due to different exchange correlation functional and method.

The calculated unit cell-resolved polarization [44] of STO is displayed in Fig. 1(b) for up and down polarization under –1% and –2% biaxial strain. Note that due to the broken crystal inversion symmetry the interfacial local polarization is asymmetric under polarization switching and is smaller than that of the bulk-like layers. Nevertheless, the layer-resolved out-of-plane polarization increases with strain.

Figure 2 shows the layer-resolved density of states (LDOS) for each layer of the Fe/STO bilayer for $P_\uparrow$ and $P_\downarrow$ under zero and –2% biaxial strain, respectively. For both spin up and

TABLE III: Spin magnetic moment, μ_s (μ_B), of the interfacial Fe and Ti atoms and orbital moment difference, $\Delta\mu_o$ ($\times 10^{-2}$ μ_B), of the interfacial Fe atom for down and up polarization for different values of biaxial strain for the Fe/$SrTiO_3$ and Fe/$BaTiO_3$ bilayers, respectively. We also list the change of the total interfacial spin moment, $\Delta\mu_s$, upon polarization reversal.

ε	$\mu_s^{\text{Ti}}(P_\downarrow)$	$\mu_s^{\text{Ti}}(P_\uparrow)$	$\mu_s^{\text{Fe}}(P_\downarrow)$	$\mu_s^{\text{Fe}}(P_\uparrow)$	$\Delta\mu_s$	$\Delta\mu_o^{\text{Fe}}(P_\downarrow)$	$\Delta\mu_o^{\text{Fe}}(P_\uparrow)$
$SrTiO_3$							
0	–0.34	–0.34	2.67	2.67	0	–0.5	–0.5
–1	–0.14	–0.41	2.71	2.61	0.37	–0.3	–0.7
–2	–0.08	–0.42	2.74	2.58	0.51	0.2	–0.8
$BaTiO_3$							
0	–0.45	–0.53	2.76	2.65	0.19	–1.8	–1.5
–1	–0.06	–0.51	2.79	2.62	0.62	–1.4	–1.2
–2	–0.03	–0.50	2.81	2.59	0.69	–0.8	–1.0
–3	0.00	–0.48	2.83	2.56	0.75	–0.3	–0.9

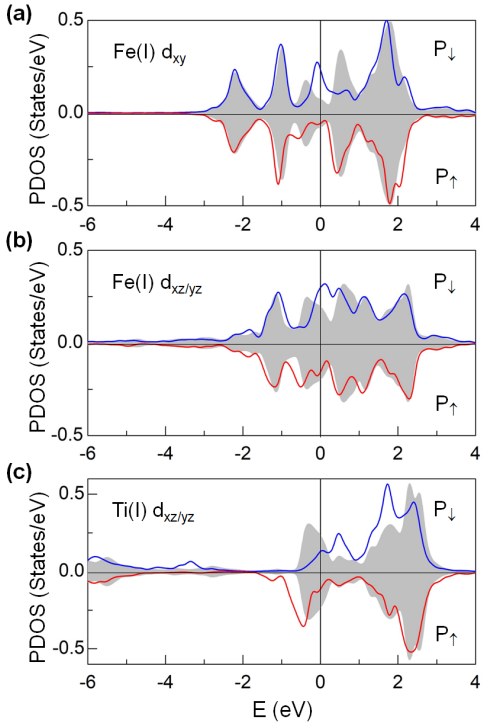

FIG. 3: (Color online) Interfacial (a) Fe d_{xy}, (b) Fe $d_{xz,yz}$, and (c) Ti $d_{xz,yz}$ PDOS of the Fe/$SrTiO_3$ bilayer for down and up polarization under zero (gray shaded area) and –2% strain (solid blue and red curves). The Fermi level is set at zero energy.

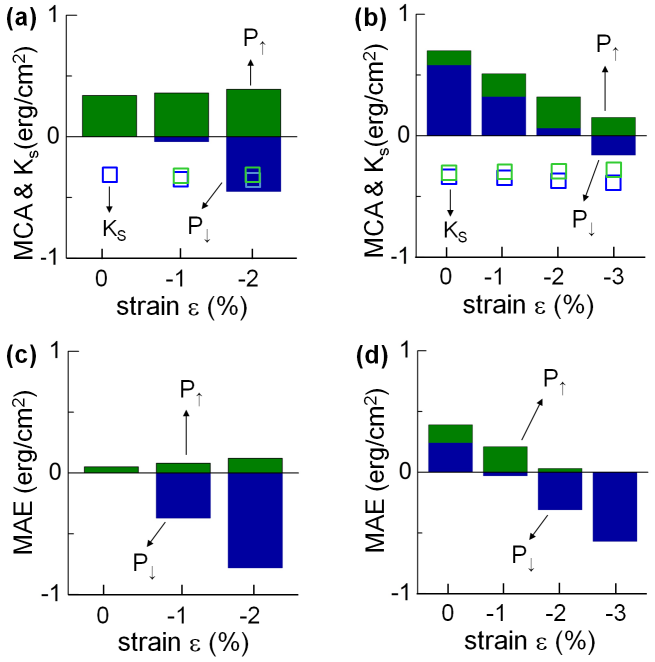

FIG. 4: (Color online) Strain dependence of magnetocrystalline anisotropy, MCA, (filled bars) and surface contribution to the shape magnetic anisotropy, K_s, (unfilled squares) for the (a) Fe/$SrTiO_3$ and (b) Fe/$BaTiO_3$ bilayer for $P_\downarrow$ (blue) and $P_\uparrow$ (green), respectively. Strain dependence of total magnetic anisotropy energy, MAE, for (c) Fe/$SrTiO_3$ and (d) Fe/$BaTiO_3$ bilayer for $P_\downarrow$ (blue) and $P_\uparrow$ (green), respectively.

down states, the Fe-derived DOS at the central and surface layers preserve those of the free-standing Fe(001) films. For the interfacial Fe, while the majority-spin LDOS are rather strain- and polarization reversal-insensitive, the minority-spin derived DOS around the Fermi level changes substantially under strain and polarization reversal. The strained DOS($P_\downarrow$) [DOS($P_\uparrow$)] near the Fermi level shifts upward [downward] in energy relative to the corresponding unstrained DOS, which in turn increases [decreases] the exchange splitting of the interfacial Fe atom. Moreover, the coincidence of these Fe peaks with the TiO_2 DOS is a reflection of the interfacial hybridization effect. Such strong hybridization gives rise to non-zero DOS at the Fermi level up to three-layer-thick deep into the STO layers due to the quantum tunneling effect. Similar results are also found in the present and previously aforementioned studies for Fe/BTO bilayer.

To better understand the origin of the strain-enhanced interfacial magnetoelectric effect we have further examined the charge transfer and orbital hybridization between the interfacial Fe and Ti d states. The minority-spin t_{2g} (d_{xy} and $d_{xz,yz}$)-projected DOS (PDOS) of the interfacial Fe and Ti atoms of the Fe/STO bilayer for down and up polarization are shown in Figs. 3(a)–3(c) for zero and –2% strain, respectively. The t_{2g} states contribute mainly to the changes of the total LDOS under strain and polarization reversal. The sensitivity of the hybridization between the interfacial Fe and Ti d states on the polarization direction causes a spin-polarized charge transfer and/or charge redistribution mainly within the interface layers. We find that under polarization switching the interfacial Fe-d_{xy} orbital looses $0.18e$ while the Fe-$d_{xz,yz}$ and Ti-$d_{xz,yz}$ orbitals gain 0.08 and $0.41e$, respectively.

Figures 4(a) and 4(b) show the contributions of the magnetocrystalline anisotropy, MCA, (blue and green bars) and the shape anisotropy, K_s, (blue and green squares) to the total magnetic anisotropy energy (MAE), for the Fe/STO and Fe/BTO bilayers, respectively, as a function of ε for $P_\downarrow$ and $P_\uparrow$. Figs. 4(c) and (d) show the total MAE for the Fe/STO and Fe/BTO bilayers, respectively, as a function of ε for $P_\downarrow$ and $P_\uparrow$. The MCA per unit interfacial area, A, is determined from $\mathrm{MCA} = [E_{[100]} - E_{[001]}]/A$, where $E_{[100]}$ and $E_{[001]}$ are the total energies with magnetization along the [100] and [001] directions, respectively. The surface/interface contribution to the shape anisotropy can be determined from Bruno's expression [45], $K_s = -(1/2)M_v M_s$, where M_v is the bulk magnetization per unit volume and M_s is the sum of *excess* surface magnetization per unit area for each layer. The calculated K_s values for the Fe/STO and Fe/BTO bilayers at zero strain are nearly identical about –0.31 erg/cm^2, and remain almost unchanged with strain and polarization.

On the other hand, for zero strain the MCA for both bilayers is positive and larger than the shape anisotropy, thus rendering the magnetization direction out of plane. For $P_\uparrow$ the MCA of

the Fe/STO remains positive and almost independent of strain ($\sim$ 0.35 erg/cm^2). In sharp contrast, the down polarization, $P_\downarrow$, reduces further the MCA from its corresponding strain-free value, resulting in a more rapid decrease of MCA with compressive strain and hence a sign reversal at $\sim$ –1%. This in turn leads to spin reorientation upon polarization reversal ($P_\downarrow \leftrightarrow P_\uparrow$) for $|\varepsilon| \geq 1\%$, as shown in Fig. 4(c). The interfacial magnetoelectric coefficient, $\beta_s = d(MAE)/dP$, thus increases with compressive strain reaching a value of about 25×10^{-3} erg/μC at –2%. For the Fe/BTO bilayer, the MCA decreases linearly with compressive strain for both $P_\uparrow$ and $P_\downarrow$, resulting in MCA reversal at $\sim$–3% due to the larger lattice constant of BTO.

This result is in contrast to previous *ab initio* calculations [29–31] of the unstrained Fe/BTO bilayer, which were not able to find a sign switching of the MCA energy via polarization reversal. Since the negative contribution of the shape anisotropy reduces the absolute value of the MCA, the total MAE changes sign even at smaller strain of about –1% similar to the Fe/STO. The large tetragonal distortion along the z-axis under strain is indeed detrimental to the perpendicular MCA, which in turn leads to the reduction of MCA. We find that the MCA values of *bulk* Fe structure are –0.04, –0.19, and –0.27 erg/cm^2 for $c/a = 1.05$ (zero strain), 1.08 (–1%), and 1.10 (–2%), respectively. Thus, for both the Fe/STO and Fe/BTO bilayers the underlying mechanism of the spin reorientation transition (discussed below) upon polarization switching is the interplay between the strain-enhanced magnetoelectric coupling associated with the enhanced polarization in the ferroelectric substrate and the strain-induced reduction of the ferromagnetic overlayer MCA.

The calculations reveal that the magnetization reorientation of the selected 3-ML Fe film under polarization reversal between –1 $\sim$ and –2% compressive strain is due to the relative small value of MAE compared to the corresponding values of other Fe film thickness. For the 2-ML Fe film previous *ab initio* calculations showed that the ground state is antiferromagnetic[30, 43]. For the 4ML-Fe/STO bilayer under –2% strain, we find that the MAE is 0.04 and 0.65 erg/cm^2 for $P_\downarrow$ and for $P_\uparrow$, respectively, suggesting that the spin reorientation via polarization reversal will occur under larger strain. Thus, the critical strain for polarization-induced magnetization switching depends on the Fe-film thickness.

The results of the strain dependence of the MCA and $\Delta\mu_o$ of the interfacial Fe atom indicate that the Bruno expression $\text{MCA} = -\frac{\xi}{4\mu_B}\Delta\mu_o$ [46], where ξ is the SOC constant, is approximately satisfied. This expression needs to be modified for structures consisting of multiple atomic species with strong hybridization and large spin-orbit interaction [47]. Nevertheless, for the Fe/STO bilayer the increase (decrease) of $\Delta\mu_o$ with strain under $P_\downarrow$ ($P_\uparrow$) correlates well with the corresponding decrease (increase) of MCA, including the sign reversal of both $\Delta\mu_o$ and MCA $\sim$ –2% under $P_\downarrow$. For the Fe/BTO bilayer the $\Delta\mu_o$ increases with strain more rapidly for $P_\downarrow$ than $P_\uparrow$, consistent with the strain- and polarization-dependence of the MCA in Fig. 4(b). Moreover, although

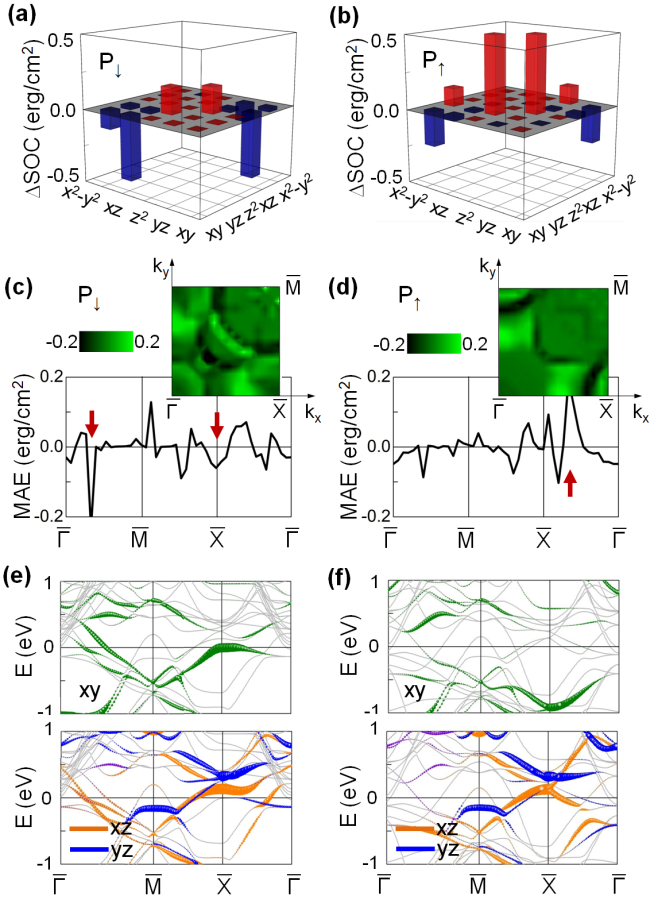

FIG. 5: (Color online) Difference of d-orbital-projected SOC energies, ΔE_{SOC}, between in- and out-of-plane magnetization orientation of the interfacial Fe atom of the Fe/SrTiO$_3$ bilayer under –2% strain for (a) $P_\downarrow$ and (b) $P_\uparrow$, respectively. (c) and (d) The corresponding **k**-resolved MCA, MCA(**k**) (in an unit of erg/cm^2), along the symmetry directions in the 2D BZ. The insets show contour plots of MAE(**k**) (in erg/cm^2) in one quarter of the 2D BZ. (e) and (f) Energy- and **k**-resolved distribution of the orbital character of the minority-spin bands of the interfacial Fe d_{xy} (upper panels) and d_{xz} and d_{yz} states (lower panels) along high symmetry direction. The Fermi level is set at zero energy.

the interfacial Ti atom exhibits nonnegligible $\Delta\mu_o$ in the range of $\sim$ 1.0–1.5$\times10^{-2}$ μ_B, depending on strain and polarization, the contribution of the Ti site to the total MAE is found to be insignificant for both Fe/STO and Fe/BTO bilayers. We find that $\xi \sim 0.2$ eV for the interfacial Fe atom in agreement with previous theoretical calculations [48], and is almost strain-independent.

In order to understand the effect of polarization reversal on the magnetic anisotropy of the interfacial Fe atom in the Fe/STO bilayer under –2% strain we show in Figs. 5(a) and 5(b) the d-orbital-projected contributions to the difference in the spin-orbit coupling (SOC) energies for in- and out-of-plane magnetization orientation, i.e., $\Delta E_{\text{soc}} = E_{\text{soc}}(\mathbf{M}^{[100]}) - E_{\text{soc}}(\mathbf{M}^{[001]})$. Here, $E_{\text{soc}} = < \frac{\hbar^2}{2m^2c^2}\frac{1}{r}\frac{dV}{dr}\mathbf{L}\cdot\mathbf{S} >$, where V(r) is the spherical part of the effective potential within the PAW

sphere, and **L** and **S** are orbital and spin operators, respectively. These expectation values are twice the actual value of the total energy correction to second order in SOC. For $P_\downarrow$ we find that the negative MCA arises primarily from the $\langle d_{xy_\downarrow}|\hat{L}_x|d_{xz_\downarrow}\rangle$ matrix elements, which deceases substantially when the polarization reverses to $P_\uparrow$ due to the absence of d_{xy}-derived states around the Fermi level [See Fig. 3(a)]. Furthermore, for $P_\uparrow$ the $\langle d_{xy_\downarrow}|\hat{L}_x|d_{xz_\downarrow}\rangle$ matrix elements yield positive contributions to the MCA of the interfacial Fe atom. Both these effects render the MCA > 0 for up polarization.

To elucidate the electronic mechanism of the strain effect on the MAE upon polarization reversal, we have calculated the k-resolved MCA according to the force theorem [49, 50]: $\mathrm{MCA}(\mathbf{k}) \approx \sum_{n\in occ}[\varepsilon(n,\mathbf{k})^{[100]} - \varepsilon(n,\mathbf{k})^{[001]}]$ in the two-dimensional Brillouin zone (2D BZ). Here, $\varepsilon(n,\mathbf{k})^{[100]([001])}$ are the eigenvalues of the Hamiltonian for magnetization along the [100] ([001]) direction. Overall, the values of MCA calculated from the force theorem are in good agreement (within 10%) with those obtained from total energy calculations. In Figs. 5(c) and 5(d) we display the $\mathrm{MCA}(\mathbf{k})$ along the symmetry directions in the 2D BZ for $P_\downarrow$ and $P_\uparrow$, respectively, for the Fe/STO bilayer under –2%, while the insets show contour plots of $\mathrm{MCA}(\mathbf{k})$ in one quarter of the 2D BZ for down and up polarizations. We find that for $P_\downarrow$ the main negative contributions to the MCA appear around $\frac{1}{3}\overline{\Gamma X}$ and at the $\overline{X}$ point, while for $P_\uparrow$ the main positive contribution appears along the $\overline{X\Gamma}$ direction.

The ferroelectric polarization reversal $P_\downarrow \rightarrow P_\uparrow$ modifies the energy landscapes of the electronic states of the ferromagnet around the Fermi level and consequently modulates the MCA. To address this point , we have employed the second-order perturbation theory of the SOC [51, 52] adopted extensively in previous *ab initio* MCA calculations [10, 11, 33, 51–54]. For the Fe thin film the majority-spin band is nearly fully occupied and hence the dominant contribution to the MCA arises from the minority-spin states. In addition, the SOC between states of opposite spin can be ignored. Therefore, within the second-order perturbation theory the MCA is determined by the SOC between occupied and unoccupied state [51]

$$MCA \propto \xi^2 \sum_{o,u} \frac{|\langle\Psi_o^\downarrow|\hat{L}_z|\Psi_u^\downarrow\rangle|^2 - |\langle\Psi_o^\downarrow|\hat{L}_x|\Psi_u^\downarrow\rangle|^2}{E_u^\downarrow - E_o^\downarrow}, \qquad (1)$$

where $\Psi_o^\downarrow$ ($E_o^\downarrow$)and $\Psi_u^\downarrow$ ($E_u^\downarrow$) are the one-electron occupied and unoccupied minority-spin states (energies) of band index n and wave vector $\mathbf{k}$ (omitted for simplicity), and $\hat{L}_{x(z)}$ is the x (z) component of the orbital angular momentum operator. We find that the strain-induced change of the MCA under polarization reversal arises primarily from changes of the band structure of the interfacial Fe atom.

In Figs. 5(e) and 5(f) we show the energy- and k-resolved distribution of the orbital character of the minority-spin bands of the interfacial Fe-derived d_{xy} and $d_{xz,yz}$ states along the high symmetry directions for $P_\downarrow$ and $P_\uparrow$ under –2% strain, respectively. The underlying origin of the negative MCA for $P_\downarrow$ around $\frac{1}{3}\overline{\Gamma X}$ and at $\overline{X}$ is the spin-orbit coupling between the minority-spin interfacial Fe-derived occupied d_{xy} states with the unoccupied d_{xz} states through the in-plane orbital angular momentum operator, $\hat{L}_x$. Upon polarization reversal $P_\downarrow \rightarrow P_\uparrow$ the negative contributions to the MCA in the aforementioned k-points decrease substantially due to the increase in energy band separation (appearing in the denominator in Eq. (1)) between the minority-spin occupied d_{xy}- and unoccupied d_{xz}-derived bands. On the other hand, the positive $\mathrm{MCA}(\mathbf{k})$ peak around the $\frac{1}{3}\overline{X\Gamma}$ for $P_\uparrow$ arises from the SOC between the interfacial Fe minority spin d_{xz}-derived states, which changed to occupied upon polarization $P_\downarrow \rightarrow P_\uparrow$ reversal, and the unoccupied d_{yz}-derived states through the out-of-plane orbital angular momentum operator, $\langle d_{xz_\downarrow}|\hat{L}_z|d_{yz_\downarrow}\rangle$. Thus, the spin reorientation upon polarization reversal is the result of the tuning of the SOC between the t_{2g} states in the vicinity of the Fermi energy due to orbital hybridization and charge redistribution effects associated with the polar TiO_2 interface.

IV. CONCLUSION

Previous theoretical studies [29–31] of the effect of electric field-induced strain (only of about 0.1 %) due to polarization switching reported a small change of MAE. In sharp contrast, our *ab initio* electronic structure calculations reveal that biaxial strains of several percent on Fe/ferroelectric bilayers grown epitaxially on various substrates have a tremendous effect on the magnetic properties leading to a spin reorientation upon polarization switching. However, direct comparison with experiment requires some caution. Further calculations of the effect of ferromagnetic film thickness, interfacial defects (oxygen and cation vacancies), cation intermixing, partial oxidation, and temperature on the MCA are required. We hope these predictions inspire further experimental explorations of exploiting percent-levels strain to harvest higher electric efficiency of magnetic anisotropy.

ACKNOWLEDGMENTS

This work was supported by NSF Grant No. ERC-TANMS-1160504 and the Basic Science Research Program through the National Research Foundation of Korea Grant No. NRF-2017R1C1B5017261.

* Electronic address: odkhuu@inu.ac.kr
† Electronic address: nick.kioussis@csun.edu

[1] W. Eerenstein, N. D. Mathur, and J. F. Scott, Multiferroic and magnetoelectric materials, Nat. Mater. **442**, 759 (2006).
[2] M. Bibes and A. Barthelemy, Towards a magnetoelectric memory, Nat. Mater. **7**, 425 (2008).
[3] Y.-H. Chu, L. W. Martin, M. B. Holcomb, M. Gajek, S.J Han, Q. He, N. Balke, C.H. Yang, D. Lee, W. Hu, Q. Zhan, P. L. Yang, A. Fraile-Fraile-Rodríguez, A. Scholl, S. X. Wang, and

R. Ramesh, Electric-field control of local ferromagnetism using a magnetoelectric multiferroic, Nat. Mater. **7**, 478 (2008).

[4] N. Spaldin, S. W. Cheong, and R. Ramesh, Multiferroics: Past, present, and future, Physics Today, **63**, 10, 38 (2010).

[5] J. T. Heron, M. Trassin, K. Ashraf, M. Gajek, Q. He, S. Y. Yang, D. E. Nikonov, Y-H. Chu, S. Salahuddin, and R. Ramesh, Electric-Field-Induced Magnetization Reversal in a Ferromagnet-Multiferroic Heterostructure, Phys. Rev. Lett. **107**, 217202 (2011).

[6] Y.-H.Chu, L. W. Martin, M. B. Holcomb, M. Gajek, S.-J. Han, Q. He, N. Balke, C.-H. Yang, D. Lee, W. Hu, Q. Zhan, P.-L. Yang, A. Fraile-Rodríguez, A. Scholl, S. X. Wang, and R. Ramesh, Electric-field control of local ferromagnetism using a magnetoelectric multiferroic, Nature Mater. **7**, 478 (2008).

[7] J. C. Slonczewski, Conductance and exchange coupling of two ferromagnets separated by a tunneling barrier, Phys. Rev. B **39**, 6995 (1989).

[8] L. Berger, Emission of spin waves by a magnetic multilayer traversed by a current, Phys. Rev. B **54**, 9353 (1996).

[9] K. L. Wang, J. G. Alzate and P. Khalili Amiri, Low-power non-volatile spintronic memory: STT-RAM and beyond, J. Phys. D: Appl. Phys. **46**, 074003 (2013).

[10] P. V. Ong, N. Kioussis, D. Odkhuu, P. K. Amiri, K. L. Wang, and G. P. Carman, Giant voltage modulation of magnetic anisotropy in strained heavy metal/magnet/insulator heterostructures, Phys. Rev. B **92**, 020407 (2015).

[11] P. V. Ong, Nicholas Kioussis, P. Khalili Amiri, and K. L. Wang, Electric-field-driven magnetization switching and nonlinear magnetoelasticity in Au/FeCo/MgO heterostructures, Scientific Reports **6**, 29815 (2016).

[12] H. Zheng, J. Wang, S. E. Lofland, Z. Ma, L. Mohaddes-Ardabili, T. Zhao, L. Salamanca-Riba, S. R. Shinde, S. B. Ogale, F. Bai, D. Viehland, Y. Jia, D. G. Schlom, M. Wuttig, A. Roytburd, R. Ramesh, Multiferroic $BaTiO_3$-$CoFe_2O_4$ Nanostructures, Science **303**, 661-663 (2004).

[13] F. Zavaliche, H. Zheng, L. Mohaddes-Ardabili, S. Y. Yang, Q. Zhan, P. Shafer, E. Reilly, R. Chopdekar, Y. Jia, P. Wright, D. G. Schlom, Y. Suzuki, and R. Ramesh, Electric Field-Induced Magnetization Switching in Epitaxial Columnar Nanostructures, Nano Lett. **5**, 1793 (2005).

[14] C. G. Duan, S. S. Jaswal, and E. Y. Tsymbal, redicted Magnetoelectric Effect in Fe/$BaTiO_3$ Multilayers: Ferroelectric Control of Magnetism Phys. Rev. Lett. **97**, 047201 (2006).

[15] S. Sahoo, S. Polisetty, C. G. Duan, S. S. Jaswal, E. Y. Tsymbal, and C. Binek, Ferroelectric control of magnetism in $BaTiO_3$/Fe heterostructures via interface strain coupling, Phys. Rev. B **76**, 092108 (2007).

[16] S. Brivio, D. Petti, R. Bertacco, and J. C. Cezar, Electric field control of magnetic anisotropies and magnetic coercivity in Fe/$BaTiO_3$ (001) heterostructures, Appl. Phys. Lett. **98**, 092505 (2011).

[17] T. Taniyama, Electric-field control of magnetism via strain transfer across ferromagnetic/ferroelectric interfaces, J. Phys.: Condens. Matter **27**, 504001 (2015).

[18] K. J. Choi, M. Biegalski, Y. L. Li, A. Sharan, J. Schubert, R. Uecker, P. Reiche, Y. B. Chen, X. Q. Pan, V. Gopalan, L.-Q. Chen, D. G. Schlom, and C. B. Eom, Enhancement of Ferroelectricity in Strained $BaTiO_3$ Thin Films, Science **306**, 1005 (2004).

[19] J. H. Haeni, P. Irvin, W. Chang, R. Uecker, P. Reiche, Y.L.Li, S. Choudhury, W. Tian, M. E. Hawley, B. Craigo, A. K. Tagantsev, X. Q. Pan, S. K. Streiffer, L. Q. Chen, S. W. Kirchoefer, J. Levy and D. G. Schlom, Room-temperature ferroelectricity in strained $SrTiO_3$, Nature **430**, 758 (2004).

[20] D. G. Schlom, L. Q. Chen, C. B. Eom, K. M. Rabe, S. K. Streiffer, and J. M. Triscone, Strain Tuning of Ferroelectric Thin Films, Annu. Rev. Mater. Res. **37**, 589 (2007).

[21] C. Ederer and N. A. Spaldin, Effect of Epitaxial Strain on the Spontaneous Polarization of Thin Film Ferroelectrics, Phys. Rev. Lett. **95**, 257601 (2005).

[22] F. He, B. O. Wells, and S. M. Shapiro, Strain Phase Diagram and Domain Orientation in $SrTiO_3$ Thin Films, Phys. Rev. Lett. **94**, 176101 (2005).

[23] A. Petraru, N. A. Pertsev, H. Kohlstedt, U. Poppe, R. Waser, A. Solbach, and U. Klemradt, Polarization and lattice strains in epitaxial $BaTiO_3$ films grown by high-pressure sputtering, J. Appl. Phys. **101**, 114106 (2007).

[24] H. N. Lee, S. M. Nakhmanson, M. F. Chisholm, H. M. Christen, K. M. Rabe, and D. Vanderbilt, Suppressed Dependence of Polarization on Epitaxial Strain in Highly Polar Ferroelectrics, Phys. Rev. Lett. **98**, 217602 (2007).

[25] M. Dawber, K. M. Rabe, and J. F. Scott, Physics of thin-film ferroelectric oxides, Rev. Mod. Phys. **77**, 1083-1130 (2005).

[26] A. V. Bune, V. M. Fridkin, S. Ducharme, L. M. Blinov, S. P. Palto, A. Sorokin, S. G. Yudin, and A. Zlatkin, Two-dimensional ferroelectric films, Nature **391**, 874-877 (1998).

[27] C. H. Ahn, K. M. Rabe, and J.-M. Triscone, Ferroelectricity at the nanoscale: local polarization in oxide thin films and heterostructures, Science **303**, 488-491 (2004).

[28] D. D. Fong, G. B. Stephenson, S. K. Streiffer, J. A. Eastman, O. Auciello, P. H. Fuoss, and C. Thompson, Ferroelectricity in ultrathin perovskite films, Science **304**, 1650 (2004).

[29] C. G. Duan, J. P. Velev, R. F. Sabirianov, W. N. Mei, S. S. Jaswal, and E. Y. Tsymbal, Tailoring magnetic anisotropy at the ferromagnetic/ferroelectric interface, App. Phys. Lett. **92**, 122905 (2008).

[30] M. Fechner, I. V. Maznichenko, S. Ostanin, A. Ernst, J. Henk, P. Bruno, and I. Mertig, Magnetic phase transition in two-phase multiferroics predicted from first principles, Phys. Rev. B **78**, 212406 (2008).

[31] M. Fechner, I. V. Maznichenko, S. Ostanin, A. Ernst, J. Henk, and I. Mertig, Ab initio study of magnetoelectricity in composite multiferroics, Phys. Status Solidi B **247**, 1600 (2010).

[32] M. K. Niranjan, J. P. Velev, C. G. Duan, S. S. Jaswal, and E. Y. Tsymbal, Magnetoelectric effect at the Fe_3O_4/$BaTiO_3$ (001) interface: A first-principles study, B **78**, 104405 (2008).

[33] D. Odkhuu, T. Tsevelmaa, S. H. Rhim, S. C. Hong, and D. Sangaa, Electric control of magnetism in low-dimensional magnets on ferroelectric surfaces, AIP Advances **7**, 055816 (2017).

[34] P. E. Blöchl, Projector augmented-wave method, Phys. Rev. B **50**, 17953 (1994).

[35] G. Kresse and J. Furthmüller, Efficient iterative schemes for ab initio total-energy calculations using a plane-wave basis set Phys. Rev. B **54**, 11169 (1996).

[36] G. Kresse and J. Furthmüller, Efficiency of ab-initio total energy calculations for metals and semiconductors using a plane-wave basis set, Comput. Mater. Sci. **6**, 15 (1996).

[37] J. P. Perdew, K. Burke, and M. Ernzerhof, Generalized Gradient Approximation Made Simple, Phys. Rev. Lett. **77**, 3865 (1996).

[38] D. D. Koelling and B. N. Harmon, A technique for relativistic spin-polarised calculations. J. Phys. C Solid State **10**, 3107 (1977).

[39] P. V. Ong and J. Lee, Strain dependent polarization and dielectric properties of epitaxial BaTiO3 from first-principles, J. Appl. Phys. **112**, 014109 (2012).

[40] R. D. King-Smith and D. Vanderbilt, Theory of polarization of crystalline solids, Phys. Rev. B **47**, 1651(R) (1993).

[41] H. L. Meyerheim, R. Popescu, N. Jedrecy, M. Vedpathak, M.

Sauvage-Simkin, R. Pinchaux, B. Heinrich, and J. Kirschner, Surface x-ray diffraction analysis of the MgO/Fe(001) interface: Evidence for an FeO layer, Phys. Rev. B **65**, 144433 (2002).

[42] St. Borek, I. V. Maznichenko, G. Fischer, W. Hergert, I. Mertig, A. Ernst, S. Ostanin, and A. Chasse, First-principles calculation of x-ray absorption spectra and x-ray magnetic circular dichroism of ultrathin Fe films on BaTiO3(001), Phys. Rev. B **85**, 134432 (2012).

[43] M. Fechner, S. Ostanin, and I. Mertig, Magnetoelectric coupling at biferroic interface studied from first principles, J. Phys.: Conf. Ser. **200** 072027 (2010).

[44] L. Wei, C. Lian, and S. Meng, Prediction of two-dimensional electron gas mediated magnetoelectric coupling at ferroelectric $PbTiO_3/SrTiO_3$ heterostructures. Phys. Rev. B **95**, 184102 (2017).

[45] P. Bruno, *Physical Origins and Theoretical Models of Magnetic Anisotropy*, *Magnetismus von Festkorpern und Grenzflochen* (Forschungszentrum Julich, Julich, 1993), vol. 24, pp. 24.1–24.28.

[46] P. Bruno, Tight-binding approach to the orbital magnetic moment and magnetocrystalline anisotropy of transition-metal monolayers. Phys. Rev. B **39**, 865 (1989).

[47] C. Andersson, B. Sanyal, O. Eriksson, L. Nordstrm, O. Karis, D. Arvanitis, T. Konishi, E. Holub-Krappe, and J. Hunter Dunn, Influence of Ligand States on the Relationship between Orbital Moment and Magnetocrystalline Anisotropy, Phys. Rev. Lett. **99**, 177207 (2007).

[48] M. Vijayakumar and M. S. Gopinathan, Spin-orbit coupling constants of transition metal atoms and ions in density functional theory, J. of Molec. Structure **361**, 15 (1996).

[49] M. Weinert, R. E. Watson, and J. W. Davenport, Total-energy differences and eigenvalue sums, Phys. Rev. B **32**, 2115 (1985).

[50] G. H. O. Daalderop, P. J. Kelly, and M. F. H. Schuurmans, First-principles calculation of the magnetocrystalline anisotropy energy of iron, cobalt, and nickel Phys. Rev. B **41**, 11919 (1990).

[51] D. S. Wang, R. Wu, and A. J. Freeman, First-principles theory of surface magnetocrystalline anisotropy and the diatomic-pair model, Phys. Rev. B **47**, 14932 (1993).

[52] G. H. O. Daalderop, P. J. Kelly, and M. F. H. Schuurmans, Magnetic anisotropy of a free-standing Co monolayer and of multilayers which contain Co monolayers, Phys. Rev. B **50**, 9989 (1994).

[53] S. Ouazi, S. Vlaic, S. Rusponi, G. Moulas, P. Buluschek, K. Halleux, S. Bornemann, S. Mankovsky, J. Minar, J. B. Staunton, H. Ebert, and H. Brune, Atomic-scale engineering of magnetic anisotropy of nanostructures through interfaces and interlines, Nat. Commun. **3**, 1313 (2012).

[54] D. Odkhuu, Electric control of magnetization reorientation in $FeRh/BaTiO_3$ mediated by a magnetic phase transition, Phys. Rev. B **96**, 134402 (2017).